Confined electron-confined phonon scattering rates in wurtzite AlN/GaN/AlN heterostructures

Evgenii P. Pokatilov and Denis L. Nika
Department of Theoretical Physics, State University of Moldova, Kishinev, Republic of Moldova

Alexander A. Balandin[a)]
Nano-Device Laboratory, Department of Electrical Engineering, University of California—Riverside, Riverside, California 92521

(Received 15 December 2003; accepted 25 February 2004)

We investigate theoretically confined electron-confined phonon scattering rates in three-layered planar wurtzite AlN/GaN/AlN heterostructures with free-surface boundary conditions. The thicknesses of the core and cladding layers are chosen to be a few nanometers to ensure phonon and electron spectrum modification due to spatial confinement. We have considered electron-phonon interactions via deformation and piezoelectric potentials. The scattering rates are calculated for both intra- and intersubband transitions of confined electrons. The influence of the built-in electric field, characteristic for GaN/AlN interfaces, on polarization and intensity of the electron-acoustic phonon interaction in heterostructures is discussed. Specific features of the deformation and piezoelectric scattering of electrons in wurtzite three-layered heterostructures and their differences from the scattering in homogenous slabs have been established. It has been shown that it is possible to tune the strength of the electron-phonon interaction in a desired way by varying the core and cladding layers thicknesses. The obtained results can be used for optimization of GaN-based heterostructures for electronic and spintronic applications.
[DOI: 10.1063/1.1710705]

I. INTRODUCTION

Spatial confinement of acoustic phonons in nanoscale structures with acoustic impedance mismatch at the boundaries can strongly affect the vibrational spectrum and modify substantially the electron-phonon interaction in comparison with bulk.[1] Nevertheless, in many cases, a three-dimensional bulk phonon approximation is still used to describe the electron-phonon interaction in hetero- and nanostructures. In this approach the Hamiltonian for the electron-phonon interaction takes into account the size quantization of the electronic states while using bulk phonon energy spectrum. The latter simplifies the theoretical treatment, since confined acoustic phonon spectra can be relatively easily found only for homogeneous structures of simple geometry, such as slabs, cylindrical, and rectangular nanowires,[1–3] or superlattices.[4] Several analytical solutions for confined phonon spectra in structures of simple geometry can be adopted from acoustics.[5] At the same time, the treatment that disregards phonon spectrum modification breaks down when the structure size becomes too small, e.g., characteristic feature size of the structure is much smaller than the phonon mean free path (MFP) at a given temperature, particularly when the elastic constant discontinuity at the nanostructure boundary is large. In this case, both the confinement of electron states and acoustic phonons should be taken into account while calculating the scattering rates.

Most of work on phonon confinement in thin films and nanowires has been done for anisotropic medium or materials with cubic lattice structure. The confined acoustic phonons in thin films (slabs) and nanowires are classified according to their spatial symmetries into shear, dilatational, and flexural polarizations.[1–3] Folded acoustic phonons in layered media have been theoretically predicted and described by Rytov.[4] The folded acoustic phonons have been later observed experimentally in quantum well superlattices.[6] More recently, acoustic phonon spectra have been calculated for regimented arrays of quantum dots from the anisotropic elasticity equation with actual elastic constants for the zinc blende dot and barrier materials.[7] The Hamiltonians of confined electron-confined phonon interaction in free standing slabs, cylindrical and rectangular quantum wires, and spherical quantum dots have been derived in Refs. 8–10. The effect of magnetic field on confined electron-confined phonon interaction in rectangular quantum wires is described in Ref. 11.

From the technological point of view, achieving acoustic phonon confinement is currently a more challenging task than achieving electron confinement. The former requires hetero- or nanostructures made of elastically dissimilar materials characterized by the large acoustic impedance mismatch or fabrication of free-standing nanostructures. Complete phonon confinement, similar to electron confinement in a quantum well with infinite potential barriers, takes place in free-standing nanostructures. Achieving strong phonon confinement and spectrum quantization is important for controlling acoustic phonon transport, e.g., *phonon engineering*,

[a)]Author to whom correspondence should be addressed; electronic mail: alexb@ee.ucr.edu

which may lead to nanoscale device applications. There have been some progress in this direction resulting in reports of fabrication and characterization of free-standing, or nearly free-standing, quantum wells, wires, and dots.[12–14] Very recently, fabrication and measurements of thermal conductivity in single crystalline free-surface Si nanowires with diameter as small as 22 nm have been reported by Li *et al.*[15] An observed strong decrease of thermal conductivity beyond the boundary scattering limit has been attributed to the phonon confinement effect, e.g., acoustic phonon modification, predicted for such structures in Ref. 16.

Heterostructures made of wurtzite GaN/AlN are very promising for electronic and optical applications due to a large direct band gap in GaN, high-temperature and high-field stability. GaN-based transistors have also demonstrated a capability for high-frequency operation with the noise levels low enough for microwave applications.[17,18] An important feature of GaN/AlN hetero- and nanostructures is the existence of a built-in electric field.[19] Spontaneous polarization, which stems from the lack of inversion symmetry, is especially large in GaN and AlN.[19,20] Owing to the lattice mismatch between GaN and AlN, the deformation appears in thin layers within GaN/AlN interface leading to the strain-induced polarization.[19,20] The built-in electric field, induced by the polarization, can reach values on the order of several MeV/cm.[20–22] It strongly affects the electron (hole) states in two-dimensional electron gas (2DEG) formed at GaN/AlN interface as well as 2DEG mobility.[23–25] In addition, the built-in electric field strongly affects light absorption and photoluminescence in GaN/AlN heterostructures.[26,27] Calculation of the intersubband and intrasubband scattering rates in GaN/AlGaN quantum wells with optical phonons participation was reported in Ref. 28. The distribution of built-in field in GaN/AlN quantum dots, which is drastically different from that in planar GaN/AlN heterostructures, has been investigated by Andreev and O'Reily[29,30] and Fonoberov and Balandin.[31,32]

In this work we present theoretical investigation of confined electron-confined phonon interaction in wurtzite AlN/GaN/AlN heterostructures. The three-layered heterostructure is chosen as a prototype of a generic thin film (quantum well) embedded within a barrier material. The considered values of the layer thickness are well below the acoustic phonon MFP at a given temperature to ensure phonon spectrum modification.

The remainder of the article is organized as follows. In the Sec. II, we describe normal acoustic phonon modes in a free-standing three-layered heterostructure. In Sec. III, the eigenmodes and eigenfunctions for electron confined within the core GaN layer are obtained. In Sec. IV, the Hamiltonians for confined electron interaction with deformation and piezoelectric potential of normal acoustic phonon modes in the considered heterostructure are derived. In Sec. V, we derive formulas for confined electron-confined phonon scattering rate in three-layered free-surface heterostructure. Results of the calculations of electron scattering rates via deformation and piezoelectric potentials for AlN/GaN/AlN heterostructure are presented in Sec. VI. Conclusions are given in Sec. VII.

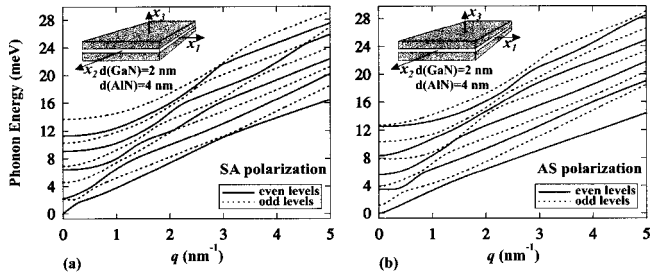

FIG. 1. Phonon energy as the function of the phonon wave vector for type A (thick barrier-thin core) heterostructure plotted for (a) SA and (b) AS polarizations.

II. CONFINED ACOUSTIC PHONON MODES IN A THREE-LAYERED HETEROSTRUCTURE

A schematic view of the considered three-layered heterostructure and basic designations are shown in the insets to Fig. 1. Axes X_1 and X_2 in the Cartesian coordinate system are in the plane of the layers while axis X_3 is perpendicular to the layer surfaces and is parallel to the hexagonal reference axis c in wurtzite lattice. The layers thicknesses are denoted by $d_i\,(i=1,2,3)$. The structure is symmetric, $d_1=d_3$, and its total thickness d is given as $d=2d_1+d_2$. The numeric calculations are performed for GaN slabs with $d_2=(2\text{ nm},10\text{ nm})$ and for the three-layered AlN/GaN/AlN heterostructures with dimensions (4 nm/2 nm/4 nm) and (2 nm/6 nm/2 nm). For the convenience of further discussion, we refer to such heterostructures as type A (thick barrier-thin core) and type B (thin barrier-thick core) heterostructures, respectively.

Details of the calculation of normal phonon modes in AlN/GaN/AlN heterostructures are described by us elsewhere.[33] The confined phonon spectra for types A and B heterostructures required for this work have been computed using the approach of Ref. 33 and the elastic constants values from Ref. 34. The normal modes with displacement vector **U** parallel to the layers do not interact with charge carriers. Therefore, these modes will not be considered in the present work. Following the notations adopted in Pokatilov *et al.*[33] the two other types of normal phonon modes are denoted as SA and AS polarizations. In the case of a slab, the SA modes correspond to dilatational modes while AS modes correspond to flexural modes.[1,8] The displacement vectors **U** for SA and AS modes lie in the $(X_3,\mathbf{q})$ plane, where **q** is a wave vector of normal vibration. The dispersion relations for type A heterostructure are shown in Fig. 1 for both SA (a) and AS (b) polarizations. One can see from these figures that only zero SA mode and zero AS mode are bulk-like. All the other modes are quantized and quasioptic in nature, e.g., $\omega(q=0)\neq 0$.

III. CONFINED ELECTRON STATES

We limit our consideration to wurtzite GaN and AlN compounds. Since wurtzite lattice lacks inversion symmetry, the heterostructure layers are spontaneously polarized. The vector of spontaneous polarization P^{sp} is oriented along the c axis. Due to the lattice constant a mismatch, $a(\text{GaN})>a(\text{AlN})$ by 2.5%, in the type A heterostructure the core

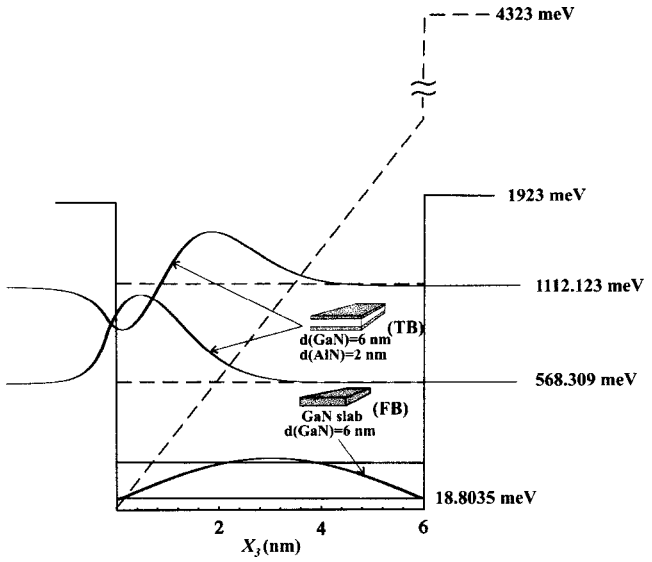

FIG. 2. Electron energy levels and electron wave functions (the ground state and the first excited states) calculated for the potential well without built-in electric potential, e.g., FB, indicated by the solid lines, and for the potential well with the built-in electric field, e.g., TB indicated by the dashed lines.

GaN layer is uniformly squeezed in the plane (X_1,X_2), while in the type B heterostructure the cladding AlN layers are stretched in the same plane. As shown in Ref. 19 such deformation does not relax for the layer thickness $d(\mathrm{GaN,AlN})<3$ nm and induces polarization P^{st}. The total polarization includes two components, e.g., $P^{\mathrm{tot}}=P^{\mathrm{sp}}+P^{\mathrm{st}}$. If the GaN core layer is relaxed (not under strain) then $P^{\mathrm{tot}}=P^{\mathrm{sp}}$. Theoretical estimates for the build-in electrostatic field F induced by total polarization P^{tot} give the value of about 10^6 V/cm.[20]

The Schrödinger equation for the transverse electron motion in the considered three-layered heterostructure can be written as

$$\left[-\frac{\hbar^2}{2}\frac{\partial}{\partial x_3}\frac{1}{m_{\parallel}(x_3)}\frac{\partial}{\partial x_3}+V_b(x_3)+V_{\text{built-in}}(x_3)\right]\psi_n(x_3)=\epsilon_{\perp n}\psi_n(x_3), \tag{1}$$

$$\epsilon_{\perp n}=E_{\perp n}-\frac{\hbar^2k^2}{2}\frac{1}{m_{\perp,n}}, \tag{2}$$

$$\frac{1}{m_{\perp,n}}=\int_{-d/2}^{d/2}|\psi_n(x_3)|^2\frac{1}{m_{\perp}(x_3)}dx_3. \tag{3}$$

Here $\hbar$ is the Plank's constant, $m_{\parallel}(x_3)$ is the effective mass of an electron along the reference axis c and $m_{\perp}(x_3)$ is the effective mass of an electron in the (X_1,X_2)-plane, $V_b(x_3)$ is the barrier potential and $V_{\text{built-in}}(x_3)=-eF_3^w x_3$, where e is the electron charge, F_3^w is the component of the built-in electrostatic field along X_3 axis in the quantum well. Equation (2) determines the energy of electron level witn quantum number n, ψ_n—is the wave function of the electron state witn a quantum number n.

In Fig. 2 the flatband ($V_{\text{built-in}}=0$; FB) potential well is depicted by the solid line while the triangular potential well (TB), which corresponds to the built-in electric field intensity $F_3^w=4$ MV/cm, is shown by the dashed line. This value of the built-in field, chosen for numeric calculations, has been adopted from Ref. 26. The energy levels (bottom of the corresponding subband) for the ground and first excited subbands in the FB and TB wells are presented in Fig. 2 with the solid and dashed lines, respectively. One can see that in the case of FB the wave function $\psi_{n=1}(x_3)$ is distributed uniformly over the layer thickness while in the case of TB the wave function $\psi_{n=1}(x_3)$ becomes strongly asymmetric and attains its maximum approximately in the distance equal to one third of the core layer thickness from the interface. This feature of the wave function results in substantial modification of the confined electron-confined phonon interaction in the case of TB as compared with the case of FB.

IV. CONFINED ELECTRON-CONFINED ACOUSTIC PHONON INTERACTION

In this section we derive the Hamiltonian for the confined electron-confined phonon interaction in a three-layered piezoelectric heterostructure. The expansion of the displacement vector over the normal modes has the form

$$\mathbf{U}(x_1,x_2,x_3)=\sum_{\alpha,s}\mathbf{U}_s^{(\alpha)}(\mathbf{r},x_3,\mathbf{q}),\quad \mathbf{r}(x_1,x_2), \tag{4}$$

where index $\alpha=$(SA,AS) indicates the polarization type and index $s=0,1,2,...N$ is the quantum number of a normal phonon mode. The displacement vector for the $(\alpha,s,\mathbf{q})$-normal mode is given by the equation

$$\mathbf{U}_s^{(\alpha)}(\mathbf{r},x_3,\mathbf{q})=\frac{1}{\sqrt{L_1L_2}}A_s^{(\alpha)}(\mathbf{q},t)\mathbf{w}_s^{\alpha}(\mathbf{q},x_3)e^{i\mathbf{qr}}, \tag{5}$$

where $A_s^{(\alpha)}$ is the oscillation amplitude and $\mathbf{w}_s^{\alpha}(\mathbf{q},x_3)$ is the polarization vector for the $(\alpha,s,\mathbf{q})$-normal mode. The polarization vector $\mathbf{w}_s^{\alpha}(\mathbf{q},x_3)$ in its turn satisfies the following orthonormal conditions:

$$\int_{-d/2}^{d/2}\mathbf{w}_s^{(\alpha)}(\mathbf{q},x_3)\rho(x_3)\mathbf{w}_{s'}^{(\alpha')}{}^*(\mathbf{q},x_3)dx_3=\rho^{(\alpha)}(q)\delta_{ss'}\delta_{\alpha\alpha'}, \tag{6}$$

where $\delta_{kk'}=0(k\neq k')$ and $\delta_{kk'}=1(k=k')$.

The Hamiltonians for interaction of an electron with $(\alpha,s,\mathbf{q})$ normal acoustic phonon mode via the deformation potential $\hat{H}_{e\text{-ph},s}^{(\alpha),d}$ and piezoelectric potential $\hat{H}_{e\text{-ph},s}^{(\alpha),p}$ are given as

$$\hat{H}_{e\text{-ph},s}^{(\alpha),\beta}=\mathrm{i}\sqrt{\frac{\hbar}{2L_1L_2\rho_s^{(\alpha)}(q)\omega_s^{(\alpha)}(q)}}\Phi_s^{(\alpha),\beta}(x_3,q)\times[b_s^{(\alpha)}(\mathbf{q})+\hat{b}_s^{\dagger(\alpha)}(-\mathbf{q})]e^{i\mathbf{qr}}, \tag{7}$$

where $\beta=(d,p)$, $\hat{b}_s^{(\alpha)}(\mathbf{q})$ is the annihilation operator, $\hat{b}_s^{\dagger(\alpha)}\times(\mathbf{q})$ is the generation operator of a phonon in $(\alpha,s,\mathbf{q})$ mode and $\Phi_s^{(\alpha),\beta}$ are the potential functions for deformation and piezoelectric scattering interactions. Functions $\rho_s^{(\alpha)}(q)$ are computed according to the orthonormal conditions of Eq. (6). The potential function for the deformation interaction is defined as

$$\Phi_s^{(\alpha),d}(x_3,q)=a_{2c}\mathbf{q}\mathbf{w}_s^{(\alpha)}(x_3,q)-a_{1c}\frac{dw_{3,s}^{(\alpha)}(x_3,q)}{dx_3}, \quad (8)$$

where a_{1c} and a_{2c} are the deformation constants for the conduction band. Numerical values of these constants were selected in line with those reported in Ref. 34. One can see from Eq. (8) that the symmetry of function $\Phi_s^{(\alpha),d}$ coincides with the symmetry of the polarization vector component $w_{1,s}^{(\alpha)}$. Thus, the even deformation potential corresponds to normal SA mode and vice versa.

The piezoelectric potential function induced by (α,s,q) acoustic phonon mode is found from the solution of the Poisson equation given by

$$\epsilon(x_3)\left[\frac{d^2\Phi_s^{(\alpha),p}(x_3,q)}{dx_3^2}-q^2\Phi_s^{(\alpha),p}(x_3,q)\right]+\frac{d\epsilon(x_3)}{dx_3}\frac{d\Phi_s^{(\alpha),p}(x_3,q)}{dx_3}=\frac{e}{\epsilon_0}\frac{d[e_{33}(x_3)w_{3,s}^{(\alpha)}(x_3,q)]}{dx_3}-\frac{e}{2\epsilon_0}e_{15}(x_3)q^2w_{3,s}^{(\alpha)}(x_3,q)-\frac{e}{\epsilon_0}q\left[\frac{e_{15}(x_3)}{2}-e_{31}(x_3)\right]\frac{dw_{1,s}^{(\alpha)}(x_3,q)}{dx_3}-\frac{e}{\epsilon_0}q\frac{de_{31}(x_3)}{dx_3}w_{1,s}^{(\alpha)}(x_3,q), \quad (9)$$

where ϵ_0 is the permittivity of free space, $e_{i,k}$ $(i=1,2,3;\ k=1,...,6)$ are the piezoelectric modules for the hexagonal crystal. Numerical values of $e_{31}(x_3)$, $e_{33}(x_3)$ are taken from Ref. 34, $e_{51}(x_3)$ are from Ref. 20 and the static dielectric constant $\epsilon(x_3)$ is from Ref. 35. Since the out-of-structure piezoelectric polarization $P_{\text{out}}^p=0$, the Maxwell boundary conditions for the piezoelectric potential function $\Phi_s^{(\alpha),p}(x_3,q)$ at the outside surface of the structure acquire the form

$$-\epsilon_0\epsilon(x_3)\left[\frac{d\Phi_s^{(\alpha),p}(x_3,q)}{dx_3}\right]_{\text{out}}=-\epsilon_0\epsilon(x_3)\left[\frac{d\Phi_s^{(\alpha),p}(x_3,q)}{dx_3}\right]_{in}-[eP_{3,s}^{(\alpha),p}]_{in}, \quad (10)$$

$$x=-\frac{d}{2}\pm 0(``+''in;``-''out)$$

or

$$x=+\frac{d}{2}\pm 0(``+''out,``-''in),$$

where $P_{3,s}^{(\alpha),p}(x_3,q)=e_{31}(x_3)qw_{1,s}^{(\alpha)}(x_3,q)-e_{33}(x_3)dw_{3,s}^{(\alpha)}\times(x_3,q)/dx_3$. It follows from Eq. (9) that the symmetry of function $\Phi_s^{(\alpha),p}$ is the same as the symmetry of the polarization vector component $w_{3,s}^{(\alpha)}$. As a result, the even piezoelectric potential corresponds to normal AS mode and vice versa.

Functions $\Phi_{s=0}^{(\text{AS}),p}$ for a GaN slab $(d=2\text{ nm})$ and for the type A heterostructure $(d=10\text{ nm})$ are shown in Fig. 3(a). Note that the functions for the GaN slab and AlN/GaN/AlN heterostructure with equal thicknesses are similar. For small phonon wave vectors q the absolute value of the function in the heterostructure with $d=10\text{ nm}$ and in the slab of the same thickness is more than the absolute value of this function in the structure with $d=2\text{ nm}$. This leads to the enhancement of piezoelectric interaction with increasing structure thickness for the electrons with relatively small momentum, e.g., for nondegenerate electron gas at low temperatures.

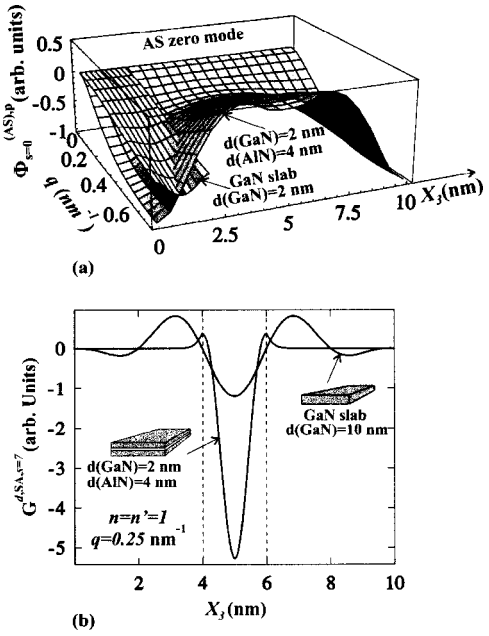

FIG. 3. (a) Piezoelectric potential for the AS zero normal mode $(s=0)$ as a function of the phonon wave vector q and coordinate x_3 shown for the slab $(0<x_3<2\text{ nm})$ and for the type A heterostructure $(0<x_3<10\text{ nm})$. (b) Integrand function $G^{d,\text{SA},s=7}(x_3)$ of the scattering rate matrix element for the deformation potential interaction in the GaN slab (10 nm) and type A heterostructure. Boundaries of the GaN heterostructure core layer are indicated by two vertical dashed lines.

V. SCATTERING RATES

The quantum mechanical probability of the system transition from the initial state i to the final state f due to electron-phonon interaction can be calculated according to Fermi's golden rule

$$\tau^{-1}(\epsilon_i)=W_{i\to f}=\frac{2\pi}{h}\sum_f |<f|H_{e\text{-ph}}|i>|^2\delta(\epsilon_f-\epsilon_i), \quad (11)$$

where summation is performed over all finite states of a system. Equation (11) determines the number of electron-phonon collisions per second, e.g., scattering rate, with which the electron transfers from some initial state i with energy ϵ_i to the finite state f with energy ϵ_f. Calculation of the relaxation time using Eq. (11) allows one to compare the intensities of electron-phonon interaction for different interaction mechanisms or, for the same mechanism, compare the scattering rates in different structures.

For the remainder of the article we will assume that the upper sign in the momentum conservation law $\mathbf{k}'=\mathbf{k}\pm\mathbf{q}$ corresponds to phonon absorption while the lower sign corresponds to phonon emission. Taking into account this conser-

vation law and, after integration over an angle in the cylindrical coordinate system, one can rewrite Eq. (11) in the following form:

$$\tau_{n,n'}^{-1}(\epsilon)=\frac{1}{2\pi\hbar^2 k}\sum_{\alpha,\beta,s} m_{\perp,n'} \times\int_0^{\infty}\frac{\left[N_s^{(\alpha)}+\frac{1}{2}\mp\frac{1}{2}\right]dq}{\rho_s^{(\alpha)}(q)\omega_s^{(\alpha)}(q)\sqrt{1-(\Delta^{\mp})^2}} \times\left[\int_{-d/2}^{d/2} G_{n,n'}^{\beta,\alpha,s}(q,x_3)dx_3\right]^2, \tag{12}$$

where $N_s^{(\alpha)}$ is the phonon equilibrium occupation number, $\omega_s^{(\alpha)}$ is the phonon frequency, and functions $\Delta^{\mp}$ and $G_{n,n'}^{\beta,\alpha,s}$ are given as

$$(\Delta^{\mp})=\frac{m_{\perp,n'}}{kq\hbar^2}\left[\epsilon_{n'}^0-\epsilon_n^0+\frac{\hbar^2k^2}{2}\left(\frac{1}{m_{\perp,n'}}-\frac{1}{m_{\perp,n}}\right)+\frac{\hbar^2q^2}{2m_{\perp,n'}}\mp\hbar\omega_s^{(\alpha)}(q)\right], \tag{13}$$

$$G_{n,n'}^{\beta,\alpha,s}(q,x_3)=\Phi_s^{(\alpha),\beta}(q,x_3)\psi_{n'}^*(x_3)\psi_n(x_3). \tag{14}$$

Note that in Eq. (12), $n=n'$ corresponds to intrasubband transitions, and $n\neq n'$ corresponds to intersubband transitions. The electron size quantization energy in heterostructures with a thickness on the order of several nanometers, is much larger than the electron thermal energy at room temperature. In this case, one can assume that only one subband ($n=1$) is occupied, and intersubband transitions are possible for the nonequilibrium system state, which can be created, for example, by optical excitation.[26,28]

The function $G_{n=1,n'=1}^{\mathrm{SA},s=7,d}(x_3, q=0.25\,\mathrm{nm}^{-1})$, is depicted in Fig. 3(b) for the GaN slab ($d=10$ nm) and for the type A heterostructure. In the slabs, the electron interacts mainly with the lowest modes ($s=0,1,2$),[8] while in the heterostructures the electron interacts intensively with all modes ($s=0,1,2,3...$). In Fig. 3(b) one can see the strength of the interaction between an electron in the ground state and seventh normal acoustic SA mode.

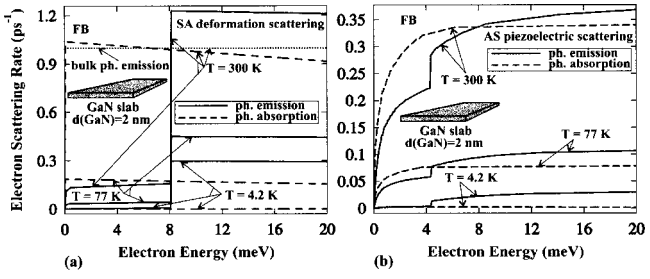

FIG. 4. Intrasubband electron scattering rate for SA normal modes as a function of the electron energy in GaN slab ($d=2$ nm) at three different temperatures of 4.2, 77, and 300 K. Solid lines correspond to phonon emission and dashed lines correspond to phonon absorption. The results are presented for the deformation potential interaction (a) and for the piezoelectric field interaction (b). For comparison, the bulk phonon emission is shown with the dotted curve.

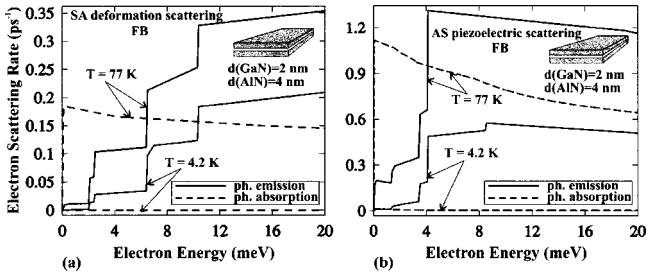

FIG. 5. Intrasubband electron scattering rate for SA normal modes as a function of the electron energy in the type A heterostructure at two different temperatures of 4.2 and 77 K. Solid lines correspond to phonon emission and dashed lines correspond to phonon absorption. The results are presented for the deformation potential interaction (a) and for the piezoelectric field interaction (b).

VI. COMPARISON OF THE SCATTERING RATES AND DISCUSSION

Calculated intrasubband scattering rates $\tau^{-1}(\epsilon)$ in GaN slab and heterostructures are presented in Figs. 4–6. In Figs. 4(a)–4(b) one can see the scattering rates in the GaN slab with the thickness $d=2$ nm. The confined electron-confined phonon scattering rates in types A and B heterostructures are shown in Figs. 5(a)–5(b) and 6(a)–6(b), respectively. One can notice in these figures that the phonon absorption processes $\tau_{\mathrm{abs}}^{-1}(\epsilon)$ are described by the smooth functions due to the fact that all phonon modes participate in the absorption process, although with different contributions determined by the value of the matrix element. The functional dependence is different for the phonon emission processes $\tau_{\mathrm{em}}^{-1}(\epsilon)$ where the well-defined steps are clearly seen at energies $\epsilon_{\mathrm{step}}=\hbar\omega_s^{(\alpha)}(q=0)$. This corresponds to the beginning of phonon emission when the phonon energy equals to the electron energy. These characteristic steps distinguish the confined electron-confined phonon scattering rates in heterostructures from the scattering rates for free electrons interacting with bulk phonons for which the relaxation rate is proportional to the square root of electron energy ϵ, i.e., $\tau^{-1}\sim(\epsilon)^{1/2}$. The calculated scattering rates are also different from the confined electron-bulk acoustic phonon scattering rates shown in Fig. 4(a) with the dotted line (phonon emission at $T=300$ K; $\tau_{\mathrm{abs}}^{-1}=\tau_{\mathrm{em}}^{-1}$). More discussion on the difference between electron-confined phonon and electron-bulk phonon scattering rates in crystals of cubic structure can be found in

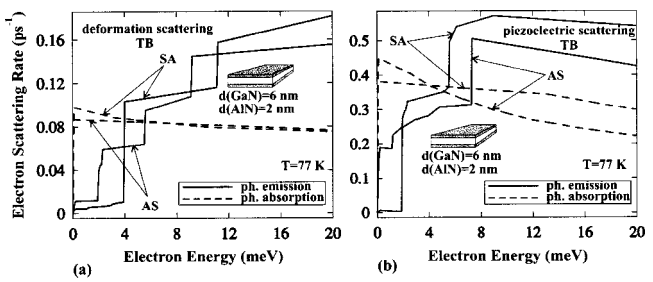

FIG. 6. Intrasubband electron scattering rate for SA and AS normal modes as a function of the electron energy in the type B heterostructure at the temperature of 77 K. Solid lines correspond to phonon emission and dashed lines correspond to phonon absorption. The results presented for the deformation potential interaction (a) and for the piezoelectric field interaction (b).

Refs. 1–3 and 8. One can also notice in Fig. 4 that since in the "thin" GaN slab with $d=2$ nm the phonon quantization is stronger than in types A and in B heterostructures with $d=10$ nm (see Figs. 5 and 6), the first steps in the thin slab are shifted to higher energies.

The number of normal modes in the heterostructure can be estimated as $d/2c_{1c}$, where c_{1c} is the lattice constant ($c_{1c}=0.51$ nm for GaN).[34] It follows from this estimate that two normal modes (bulk like $s=0$ and quantized $s=1$) of each polarizations (SA and AS) are in the thin GaN slab, whereas ten normal modes of SA and AS polarizations are in both types A and B heterostructures (including two modes with $s=0$, which are bulk like). The distinctive feature of scattering rates $\tau^{-1}(\epsilon)$ in heterostructures is the involvement of the higher phonon modes into the emission processes. Figure 3(b) shows that higher phonon modes in heterostructures intensively interact with electrons due to confinement of the electron in the heterostructure core layer. In the type B heterostructure the electron wave function is shifted to the heterostructure surface by the built-in electric field. Therefore, the symmetry with respect to the central plane is broken. As a result, the electron deformation potential interaction with AS modes and the electron piezoelectric interaction with SA modes emerge, while the deformation potential interaction with SA modes and the piezoelectric interaction with AS modes become weaker. Note that in the type A heterostructure, the built-in electric field does not practically influence the value of $\tau^{-1}(\epsilon)$ because of the small potential bias.

The dependence of the scattering rate on the nanostructure thickness [see Figs. 4(a) and 5(a)] is a manifestation of the size quantization effect in electron-phonon interaction. There is no such effect in bulk because of the increase in the number of normal acoustic modes, which is proportional to V (where V is the sample volume) and is compensated by the decrease in their amplitudes $\sim V^{-1/2}$ while computing the scattering rate τ^{-1}. Analogously, in nanostructures the number of normal acoustic modes increases as $\sim d$ and the amplitude of each modes decreases as $\sim d^{-1/2}$. At the same time, the efficiency of the deformation potential interaction of electrons with the higher normal acoustic phonon modes in a thicker heterostructure is weakened (see Fig. 5). As a result, the scattering rate decreases with increasing thickness d [compare Figs. 4(a) and 5(a)].

The piezoelectric potential interaction is a long-distance interaction. To estimate its dependence on the structure thickness, we can write, using Eq. (9), the following expression $|\Phi^{p,d}|\sim d|w_s^{(\alpha)}|\sim d^{1/2}$. This general dependence can be strongly modified by the change of the sign of the function $\Phi_s^p(x_3,q)$ for large values of s and q. Comparing Fig. 4(b) with Fig. 5(b) one can see that the increase of the structure thickness leads to the enhancement of the piezoelectric interaction.

Optical excitation of electrons into the first exited subband followed by relaxation to the ground state subband can be characterized by the function $\tau_{21}^{-1}(\epsilon)$. This function is shown in Fig. 7(a). The reverse process, due to thermal excitation, is described by the function $\tau_{12}^{-1}(\epsilon)$ [see Fig. 7(b)]. The main contribution to these transitions comes from the

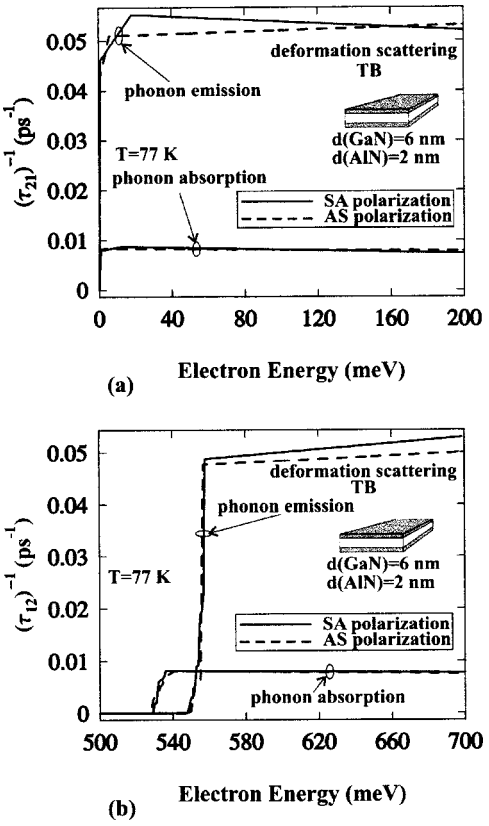

FIG. 7. Intersubband electron sattering rate for SA and AS normal modes as a function of the electron energy in the type B heterostructure at the temperature of 77 K. Solid lines correspond to SA modes while dashed lines correspond to AS modes. Panel (a) shows transitions from the excited to the ground state: 2→1; while panel (b) shows transitions from the ground to the excited state: 1→2.

deformation potential interaction owing to the large value of the electron momentum. The total relaxation rates, e.g., absorption and emission processes together, $\tau^{-1}(\text{abs}+\text{em})$ are shown in Fig. 8(a). The average total relaxation rates $\tau_{\text{tot}}^{-1}(T)=\Sigma_{\alpha,\beta}[\tau^{-1}(T)]^{(\alpha),\beta}$ obtained by averaging of $[\tau^{-1}(\epsilon)]^{(\alpha),\beta}$ using the Maxwell distribution for non-degenerate electrons are presented in Fig. 8(b). The resulting inequalities $\tau_{\text{tot}}^{-1}(T,\text{type A})>\tau_{\text{tot}}^{-1}(T,\text{type B})>\tau_{\text{tot}}^{-1}(T,10\text{ nm,slab})>\tau_{\text{tot}}^{-1}(T,2\text{ nm,slab})$ are explained by the reasons stated earlier. In brief they can be formulated as follows: (i) inclusion of the higher normal modes in the scattering processes in heterostructures and (ii) enhancement of the piezoelectric potential interaction ($\sim d^{1/2}$) and weakening of the deformation potential interaction ($\sim d^{-1/2}$) with the increasing layer thickness d. In the structures without piezoelectric polarization the inequalities are different from the previous case and are given as $\tau_{\text{tot}}^{-1}(T,2\text{nm,slab})>\tau_{\text{tot}}^{-1}(T,\text{type A})>\tau_{\text{tot}}^{-1}(T,\text{type B})>\tau_{\text{tot}}^{-1}(T,10\text{ nm,slab})$.

VII. CONCLUSIONS

We have theoretically investigated confined electron-confined phonon scattering rates in thin three-layered wurtzite AlN/GaN/AlN heterostructures. The dependence of the deformation potential and piezoelectric potential scattering rates on electron energy, temperature, and layer thickness has

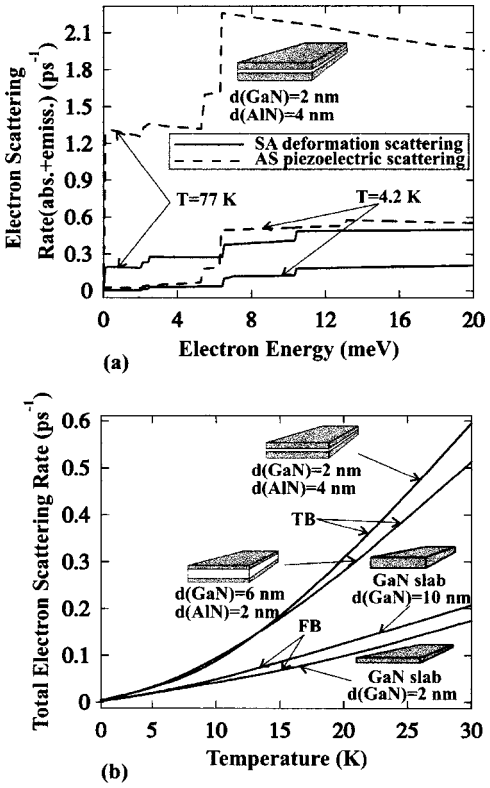

FIG. 8. (a) Combined (absorption+emission) intrasubband electron scattering rate as a function of the electron energy in the type A heterostructure at two different temperatures of 4.2 and 77 K. Solid lines correspond to the deformation potential interaction of SA normal modes and dashed lines correspond to the piezoelectric field interaction of AS normal modes. (b) Total confined electron-confined phonon scattering rate obtained by integration over all polarizations for both deformation potential and piezoelectric field interactions as a function of temperature. The results are shown for two different slab thicknesses ($d=2$ nm and $d=10$ nm) and two different heterostructures: type A (4 nm/2 nm/4 nm) and type B (2 nm/6 nm/2 nm).

been obtained. It is established that in thin three-layered wurtzite heterostructures the electrons have stronger coupling to the high-energy phonon modes than in the slabs. This effect may be useful in design of high-frequency GaN-based devices when a fast electron relaxation is required. It has also been observed that in thicker heterostructures the built-in electric field enhances electron interaction with AS phonon modes via deformation potential and with SA phonon modes via piezoelectric potential. At the same time, the total scattering rate $\tau_{SA}^{-1}+\tau_{AS}^{-1}$ remains approximately constant with the variation of the built-in electric field. In the considered heterostructures piezoelectric interaction plays the main role in the intrasubband scattering while the deformation potential interaction dominates the intersubband scattering. The results obtained for confined electron-confined phonon interaction in wurtzite AlN/GaN/AlN thin heterostructures extend the concept of phonon engineering and can be used for optimization of GaN-based electronic and spintronic devices.

ACKNOWLEDGMENTS

The work in UCR has been supported in part by the ONR Project No. N00014-02-1-0352 and NSF Early Faculty CAREER Development award to A.A.B. The work in SUM has been supported in part by the U.S. CRDF Project No. MP2-3044. The authors acknowledge Dr. V. A. Fonoberov and A. Morgan (Nano-Device Laboratory, UCR) for valuable comments on the manuscript.

[1] N. Bannov, V. Mitin, and M. Stroscio, Phys. Status Solidi B **183**, 131 (1994).
[2] V. G. Grigoryan and D. G. Sedrakyan, Akust. Zh. **29**, 470 (1983).
[3] N. Nishiguchi, Y. Ando, and M. Wybourne, J. Phys.: Condens. Matter **9**, 5751 (1997).
[4] S. M. Rytov, Akust. Zh. **2**, 71 (1956) [Sov. Phys. Acoust. **2**, 67 (1956)].
[5] *Physical Acoustic*, edited by W. P. Meson (Academic, New York, 1964), Vol. I, Part A.
[6] C. Colvard, T. A. Gant, M. V. Klein, R. Merlin, R. Fisher, H. Morkoc, and A. C. Gossard, Phys. Rev. B **31**, 2080 (1985).
[7] L. O. Lazarenkova and A. A. Balandin, Phys. Rev. B **66**, 245319 (2002).
[8] N. Bannov, V. Aristov, V. Mitin, and M. A. Stroscio, Phys. Rev. B **51**, 9930 (1995).
[9] M. A. Stroscio, K. W. Kim, S. G. Yu, and A. Ballato, J. Appl. Phys. **76**, 4670 (1994).
[10] S. G. Yu, K. W. Kim, M. A. Stroscio, G. J. Iafrate, and A. Ballato, Phys. Rev. B **50**, 1733 (1994).
[11] A. Svizhenko, A. Balandin, S. Bandyopadhyay, and M. Stroscio, Phys. Rev. B **57**, 4687 (1998).
[12] M. Williams, S. Shunk, M. Young, D. Docter, D. Tennant, and B. Miller, Appl. Phys. Lett. **61**, 1353 (1992).
[13] K. Yoh, A. Nishida, H. Kunitomo, T. Ogura, and M. Inoue, Jpn. J. Appl. Phys., Part 1 **32**, 6237 (1993).
[14] M. Foad, C. Wilkinson, C. Dunscomb, and R. Williams, Appl. Phys. Lett. **60**, 2531 (1992).
[15] D. Li, Y. Wu, P. Kim, L. Shi, P. Yang, and A. Majumdar, Appl. Phys. Lett. **83**, 2934 (2003).
[16] J. Zou and A. Balandin, J. Appl. Phys. **89**, 2932 (2001); A. Balandin and K. L. Wang, Phys. Rev. B **58**, 1544 (1998).
[17] A. Balandin, S. V. Morozov, S. Cai, R. Li, K. L. Wang, G. Wijeratne, and C. R. Viswanathan, IEEE Trans. Electron Devices **47**, 1413 (1999).
[18] M. E. Levinshtein, S. L. Rumyantsev, R. Gaska, J. W. Yang, and M. S. Shur, Appl. Phys. Lett. **73**, 1089 (1998).
[19] A. Bykhovski, B. Gelmont, and M. Shur, J. Appl. Phys. **74**, 6734 (1993); **78**, 3691 (1995); **81**, 6332 (1997).
[20] F. Bernardini, V. Fiorentini, and D. Vanderbilt, Phys. Rev. B **56**, R10024 (1997); F. Bernardini and V. Fiorentini, *ibid.* **57**, R9427 (1998).
[21] C. Adelman, E. Sarigiannidou, D. Jalabert, Y. Hori, J.-L. Rouviere, and B. Daudin, Appl. Phys. Lett. **82**, 4154 (2003).
[22] N. Grandjean, B. Damilano, S. Dalmasso, M. Leroux, M. Laught, and J. Massies, J. Appl. Phys. **86**, 3714 (1999).
[23] L. Hsu and W. Walukiewicz, Appl. Phys. Lett. **76**, 339 (1998); J. Appl. Phys. **89**, 1783 (2001).
[24] S.-H. Park and S.-L. Chuang, J. Appl. Phys. **87**, 353 (2000).
[25] L. Hsu and W. Walukiewicz, Phys. Rev. B **56**, 1520 (1997).
[26] N. Suzuki and N. Iizuka, Jpn. J. Appl. Phys., Part 2 **38**, L363 (1999).
[27] M. Leroux, N. Grandjean, J. Massies, B. Gil, P. Lefebvre, and P. Bigenwald, Phys. Rev. B **60**, 1496 (1999).
[28] S.-H. Park, D. Ahn, and Y.-T. Lee, Jpn. J. Appl. Phys., Part 2 **40**, L941 (2001).
[29] A. D. Andreev and E. P. O'Reilly, Nanotechnology **11**, 256 (2000).
[30] A. D. Andreev and E. P. O'Reilly, Phys. Rev. B **62**, 15851 (2000).
[31] V. A. Fonoberov and A. A. Balandin, J. Appl. Phys. **94**, 7178 (2003).
[32] V. A. Fonoberov, E. P. Pokatilov, and A. A. Balandin, J. Nanosci. Nanotechnol. **3**, 253 (2003).
[33] E. P. Pokatilov, D. L. Nika, and A. A. Balandin, Superlattices Microstruct. **33**, 155 (2003).
[34] I. Vurgaftman, J. R. Meyer, and L. R. Ram-Mohan, J. Appl. Phys. **89**, 5815 (2001).
[35] V. Bougrov, M. Levinshtein, S. L. Rumyantsev, and A. Zubrilov, in *Properties of Advanced Semiconductor Materials*, edited by M. E. Levinshtein, S. L. Rumyantsev, and M. S. Shur (Wiley, Inc., New York, 2001).